A&A 519, A86 (2010)
DOI: 10.1051/0004-6361/201014031

Astronomy & Astrophysics

Search for broad absorption lines in spectra of stars in the field of supernova remnant RX J0852.0-4622 (Vela Jr.)

A. F. Iyudin[1,2], Yu. V. Pakhomov[3], N. N. Chugai[3], J. Greiner[1], M. Axelsson[4], S. Larsson[4], and T. A. Ryabchikova[3]

[1] Max-Planck-Institut für extraterrestrische Physik, Postfach 1312, 85741 Garching, Germany
e-mail: ani@mpe.mpg.de
[2] Skobeltsyn Institute of Nuclear Physics, Moscow State University, Vorob'evy Gory, 119992 Moscow, Russian Federation
[3] Institute of Astronomy, RAS, Pyatnitskaya 48, 119017, Moscow, Russian Federation
[4] Stockholm University, AlbaNova University Center, Department of Astronomy, 106 91 Stockholm, Sweden

Received 9 January 2010 / Accepted 24 May 2010

ABSTRACT

Aims. Supernova remnant (SNR) RX J0852.0-4622 is one of the youngest and is most likely the closest among known Galactic SNRs. It was detected in X-rays, the ^{44}Ti γ-line, and radio. We obtain and analyze medium-resolution spectra of 14 stars in the direction towards the SNR RX J0852.0-4622 in an attempt to detect broad absorption lines of unshocked ejecta against background stars.

Methods. Spectral synthesis is performed for all the stars in the wavelength range of 3740−4020 Å to extract the broad absorption lines of Ca II related to the SNR RX J0852.0-4622.

Results. We do not detect any broad absorption line and place a 3σ upper limit on the relative depths of <0.04 for the broad Ca II absorption produced by the SNR. We detect narrow low and high velocity absorption components of Ca II. High velocity $|V_{\rm LSR}| \sim 100-140$ km s^{-1} components are attributed to radiative shocks in clouds engulfed by the old Vela SNR. The upper limit to the absorption line strength combined with the width and flux of the ^{44}Ti γ-ray line 1.16 MeV lead us to conclude that SNR RX J0852.0-4622 was probably produced by an energetic SN Ic explosion.

Key words. line: formation – stars: fundamental parameters – stars: distances – ISM: supernova remnants – supernovae: general – supernova: individual: RX J0852.0-4622

1. Introduction

Young supernova remnants (SNRs) at the deceleration stage generally provide us with an opportunity to probe the supernova (SN) ejecta not yet polluted by the circumstellar matter (CSM). The ejecta composition and structure are usually studied by analyzing the X-ray spectra emanating from the reverse shock. In some young SNRs related to core-collapse SNe, e.g., Cas A, the optical emission of undecelerated ejecta clumps are observed when they penetrate the post-shock layer, in which case they are powered by slow radiative shocks. Unshocked ejecta material is cold and does not radiate, thus remaining invisible in emission.

However, in rare cases the unshocked ejecta of SNR can be observed in resonance absorption lines against a background light source seen through the SNR shell. Among Galactic SNR, this method has been applied successfully only to SN 1006, where the ejecta was observed in the ultraviolet absorption lines against the spectra of hot stars and QSOs (Hamilton et al. 1997; Winkler et al. 2005; Hamilton et al. 2007). There is also one extragalactic SNR detected in absorption lines: the remnant of SN 1885 in M 31. It was first detected by ground-based imaging in Fe I 3860 Å band against the M 31 bulge (Fesen et al. 1989) and afterwards by *HST* imaging and spectroscopy (Fesen et al. 1999). The optical spectrum of this SNR contains strong Fe I, Ca II, and Ca I broad resonance absorption lines produced by the unshocked ejecta.

RX J0852.0-4622 (Vela Jr., G266.2-1.2) is a young galactic SNR detected by means of its emission in hard X-rays (Aschenbach 1998), the ^{44}Ti 1.16 MeV γ-ray line (Iyudin et al. 1998), radio (Duncan & Green 2000), and TeV γ-rays (Aharonian et al. 2005). Vela Jr. with a diameter of ~2° is superimposed on the eastern part of the well-known old Vela SNR. The age and distance of Vela Jr. are estimated to 700 ± 150 yr and ~200 pc, respectively (Aschenbach et al. 1999; Bamba et al. 2005). The age, distance, and angular radius imply an average expansion velocity of ~5000 km s^{-1}.

Using *XMM-Newton* images, Katsuda et al. (2008) measured the proper motion of the bright NW rim of RX J0852.0-4622. The derived value turns out to be about 5 times lower than the predicted average expansion rate of Vela Jr. On the basis of the measured proper motion, Katsuda et al. (2008) estimate the age of Vela Jr. to be 1700−4300 years and its distance to be ~750 pc. Although the conclusion could be hampered by a possible interaction with the recently encountered dense interstellar medium, the possibility of a large age cannot presently be fully ruled out.

Given the uncertainty in the age issue, we should carefully study the implications of a young age. In this respect, it is tempting to consider the unshocked ejecta of Vela Jr. using absorption spectroscopy against background stars. Our preliminary estimates showed that broad Ca II absorption lines might be observed. Here we report results of spectral observations and analysis of the spectra of distant stars across the Vela Jr. In Sect. 2, we describe the observations and data reduction. The results of the spectral synthesis and extraction of broad and interstellar Ca II absorption are presented in Sect. 3. We fail identify any broad absorption lines and the implications of this are discussed in Sect. 4.

Table 1. List of the observed stars.

N	Star	RA (2000.0)	Dec	V (mag)	Sp	$B-V$) (mag)	p	S/N	σ
1	HD 75309	08 47 28.0	–46 27 04	7.84	B2Ib/II	0.01	0.79	270	0.008
2	HD 75820	08 50 26.0	–46 14 53	8.64	B9V	−0.02	0.27	260	0.007
3	HD 75873	08 50 48.8	–46 18 36	8.10	A3II/III	0.38	0.20	160	0.010
4	HD 75955	08 51 26.0	–45 37 23	7.73	B9V	−0.01	0.67	240	0.005
5	HD 75968	08 51 32.8	–46 36 36	8.14	B9III/IV	−0.12	0.33	200	0.006
6	HD 76060	08 52 02.4	–46 17 20	7.88	B8IV/V	−0.09	0.02	350	0.005
7	HD 76589	08 55 23.0	–46 53 28	8.34	B9IV	−0.05	0.84	270	0.009
8	HD 76649	08 55 50.4	–46 20 30	8.33	B7II/III	0.14	0.67	150	0.008
9	HD 76744	08 56 18.2	–46 19 57	8.69	A0V	0.08	0.75	200	0.009
10	CD-454590	08 49 35.5	–46 23 18	9.58	B5	0.20	0.42	140	0.010
11	CD-454606	08 50 15.0	–45 31 22	8.96	B0.5V	0.38	0.82	180	0.009
12	CD-454645	08 51 34.9	–46 09 54	10.32	A0	0.20	0.14	90	0.012
13	CD-454676	08 53 22.0	–46 02 09	8.93	B0.5III	0.77	0.35	140	0.014
14	CD-464666	08 50 44.3	–46 38 11	9.81	A0II	0.60	0.40	90	0.009

2. Observations and data reduction

Spectra were obtained on the ESO 3.6-m telescope NTT (program 080.D-0012(A) PI: A.F. Iyudin) using the echelle spectrograph EMMI in BLMD mode of medium-dispersion spectroscopy with holographic grating #11 (3000 grooves/mm and maximum light reflectivity at $\lambda_{\rm blaze}$ = 3500 Å). The dispersion is 0.15 Å/pix, the resolving power is $\lambda/\Delta\lambda$ = 9000 for a slit width of 1.02″ and a registered wavelength band of ∼1500 Å. The signal-to-noise ratio (S/N) is between 90 and 350. For each star, two overlapped spectra in the range of 3740−4021 Å were obtained with centers at 3820 Å and 3945 Å. This spectral region encompasses resonance spectral lines of Fe I (3860 Å) and Ca II (3933 Å, 3968 Å).

Among the observed stars, ten are of B-type and four of A-type (Table 1) with magnitudes $7^{\rm m} < V < 11^{\rm m}$. Table 1 contains the star number, star HD/CD name, right ascension, declination, V-magnitude, spectral type, $B-V$ color index, relative impact parameter p, and signal-to-noise ratio (S/N), and 1σ, which represents the root mean square error in the spectral fit (see Sect. 3). The impact parameter is defined as $p = \theta/\rho$, where θ is the angular distance of the star from the SNR center and ρ = 1° is the SNR angular radius. The SNR center presumably coincides with the neutron star candidate AX J0851.9-4617 (Slane et al. 2001), which has coordinates $({\rm RA, Dec})_{2000}$ = ($08^{\rm h}51^{\rm m}57^{\rm s}$, −46°17′.4). The preliminary estimated distances of selected stars are in the range between 240−2000 pc, so at least some of the stars lie behind Vela Jr. Positions of all stars of the program across the Vela Jr. X-ray image (Rosat All Sky Survey data with energies above 1.3 keV) and TeV γ-ray image (Aharonian et al. 2005) are shown in Fig. 1.

Preliminary processing of the spectral CCD images, extracting the spectra, and performing wavelength calibration using ThAr-lamp data were all completed by employing the EMMI native *emmi_quickred* script of MIDAS; the atmosphere and interstellar extinction was also taken into account for each individual star. The spectra are flux calibrated with the help of spectra of the standard star HD 60753 taken in the same set of observations. This star has a calibrated flux in the UV band only. The visual flux is synthesized applying Kurucz ATLAS9 code (Kurucz 1993) and SynthVb package (Tsymbal et al. 2003). A stellar atmosphere model is calculated for solar metallicity, effective temperature $T_{\rm eff}$ = 16 200 K (σ = 150 K), gravity $\log g$ = 3.56 (σ = 0.05), rotation velocity $V \sin i$ = 24 km s^{-1}(σ = 2 km s^{-1}), and interstellar absorption A_V = 0.25 (σ = 0.03). The

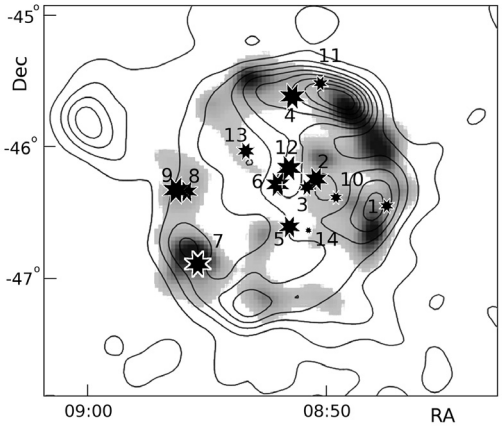

Fig. 1. Positions of the stars across the SNR images taken in TeV γ-rays (grayscale) and in hard X-rays (contours). The star numbers correspond to those in the first column of Table 1. The cross is the position of the neutron star AX J0851.9-4617. The size of symbols qualitatively reflects the distance with the largest symbol being closest star.

derived response function is used to produce flux-calibrated stellar spectra. One should emphasize that this procedure provides us with the precise relative flux across a wide wavelength range but not the absolute flux; the latter, in fact, is not needed for our purposes.

3. Analysis of spectra

The obtained stellar spectra were analyzed by applying a synthetic flux calculation employing the SynthVb and ATLAS9 codes to derive the stellar parameters $T_{\rm eff}$, $\log g$, and $V \sin i$ (Table 2). To determine the rotation velocity, we use a standard method based on Fourier transformation of profiles of weak spectral lines (Carroll 1933). We adopted the limb darkening parameter ϵ = 0.6.

The parameters of stellar atmosphere models were found by fitting the synthesized profiles to six Balmer lines (H7-H12). The fitting procedure includes multiplication of the observed spectra by a fitting factor $C(\lambda)$, which is defined as the linear approximation to the ratio of synthetic to observed spectrum $F_{\rm l}^{\rm syn}/F_{\rm l}^{\rm obs}$. In this case, we do not introduce any nonlinear distortion into the

Table 2. Parameters of the stars and distances calculated by spectral method and from Hipparcos parallax.

Star	$T_{\rm eff}$ (K)	$\log g$	$V \sin i$ (km s^{-1})	$V_{\rm r}$ (km s^{-1})	$(B-V)_0$ (mag)	A_V (mag)	M ($M_\odot$)	$d_{\rm sp}$ (pc)	$d_{\rm HIP}$ (pc)
HD 75309	26 500 ± 400	3.60 ± 0.10	210	43	–0.25	0.8	16	1900 ± 300	
HD 75820	11 400 ± 200	4.00 ± 0.10	200	31	–0.10	0.2	3.2	470 ± 100	505 ± 184
HD 75873	8900 ± 200	2.50 ± 0.05	15	41	0.01	1.2	6	1400 ± 200	
HD 75955	10 400 ± 200	3.85 ± 0.10	190	24	–0.07	0.2	3.0	320± 70	262± 35
HD 75968	12 250 ± 150	3.86 ± 0.05	80	35	–0.11	0.0	3.8	570 ± 140	719 ± 254
HD 76060	13 400 ± 200	4.10 ± 0.10	240	36	–0.13	0.1	3.6	390± 90	335± 63
HD 76589	11 800 ± 200	4.10 ± 0.10	95	0	–0.10	0.1	3.2	390± 90	240± 76
HD 76649	13 300 ± 150	3.65 ± 0.05	33	33	–0.13	0.8	4.5	640 ± 110	
HD 76744	10 500 ± 200	4.20 ± 0.10	150	–7	–0.08	0.5	2.4	270± 50	
CD-454590	22 400 ± 400	3.60 ± 0.10	140	31	–0.22	1.3	11	2400 ± 300	
CD-454606	29 500 ± 500	3.80 ± 0.10	240	33	–0.27	2.0	17	1670 ± 160	
CD-454645	8400 ± 200	4.35 ± 0.10	80	35	0.08	0.4	1.8	330± 70	
CD-454676	29 000 ± 500	3.70 ± 0.10	125	20	–0.27	3.2	18	1080 ± 150	
CD-464666	10 500 ± 200	2.05 ± 0.05	30	49	–0.08	2.1	12	5700 ± 500	

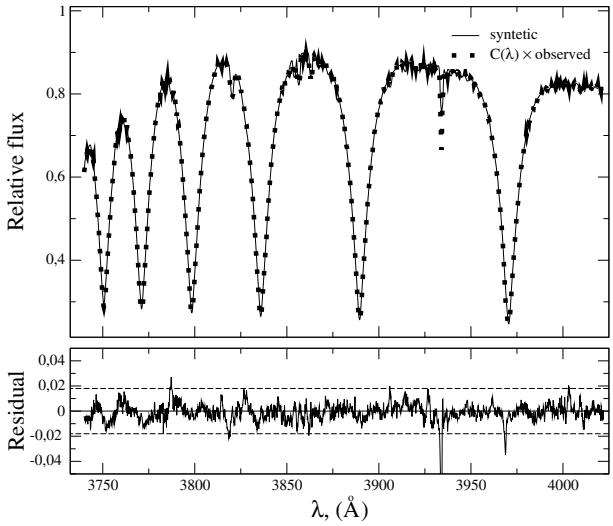

Fig. 2. Observed spectrum of the star HD 75968, synthetic spectrum, and the residual spectrum with 3σ error box

observed spectrum. The best fit is attained by minimizing the relative residual flux between the observed and synthetic spectrum

$$r = \frac{C(\lambda) * F_{\rm l}^{\rm obs} - F_{\rm l}^{\rm syn}}{F_{\rm c}^{\rm syn}}, \quad (1)$$

where $F_{\rm c}^{\rm syn}$ is the continuum flux of the synthetic spectrum. Using the relative flux permits us to avoid problems related to a poorly defined observed continuum. An example of the fit quality is demonstrated by Fig. 2. The 1σ statistical error in the spectral fit for individual stars are given in the last column of Table 1. Any interstellar lines with an intensity exceeding the 3σ error, which lie in the range of 1.5–4.2%, should be visible in the residual spectra. As an example, the residual spectrum of star HD 75968 (Fig. 2) appeanrs to contain the Ca II interstellar absorption doublet. We believe that the systematic errors in producing residual spectra are smaller than the quoted 3σ statistical error.

3.1. Interstellar reddening and distance estimate

Interstellar reddening in the observed spectra is taken into account using extinction data reported by Mathis (1990). In the first step, we determine stellar parameters and calculate normal color indexes $(B-V)_0$ (Castelli & Kurucz 2003). We then use the observed $(B-V)$ to derive color excess $E(B-V)$ and V-band absorption, $A_V = 3.1E(B-V)$. At the second step, we improve our determination of the stellar atmosphere parameters and recalculate the reddening.

To determine distances, we employ a modified method of spectral parallaxes in which the stellar luminosity is derived from stellar evolutionary tracks as follows. Using stellar parameters ($T_{\rm eff}$ and $\log g$) and evolutionary tracks (Schaller et al. 1992), we estimate the stellar mass and thus derive the bolometric luminosity. The absolute magnitude M_V is then determined using the bolometric correction taken from (Bessell et al. 1998). The luminosity and distance are thus determined from the standard formulae

$$\log L = -10.607 + \log(M/M_\odot) + 4\log T_{\rm eff} - \log g, \quad (2)$$

$$M_V = 4.69 - 2.5\log L - BC_V, \quad (3)$$

$$\log d_{\rm sp} = 0.2(M_V - m_V - 5 + A_V). \quad (4)$$

The normal color index $(B-V)_0$, interstellar absorption A_V, stellar masses M, and distances are listed in Table 2. In the last column, we also indicate the available distances according to HIPPARCOS parallaxes (van Leeuwen 2007). The distances determined by both methods agree within errors (Fig. 3), which supports the reliability of distances obtained by the method of spectral parallax.

3.2. Interstellar lines

The relative residual spectra for all the stars are shown in Fig. 4. The 3σ levels are also indicated for each star. Large values of 3σ are seen for late B and A type stars with low rotation speeds due to problems in fitting narrow stellar spectral lines using the accepted solar abundance of chemical elements. The spectra do not uncover broad absorption resonance lines of Ca II 3933 Å, 3968 Å, or Fe I 3860 Å. In particular, the relative depth of the broad Ca II absorption (if any) produced by Vela Jr. is smaller than 0.04 at the level of 3σ. We note, that the weak absorption at 3819 Å and 4009 Å in the hottest stars of our sample are related to helium lines, which are generally affected by non-LTE excitation and cannot be modeled reliably in the LTE approximation.

With the exception of two stars (HD 75873 and CD-454645), all the spectra contain narrow unresolved interstellar Ca II lines;

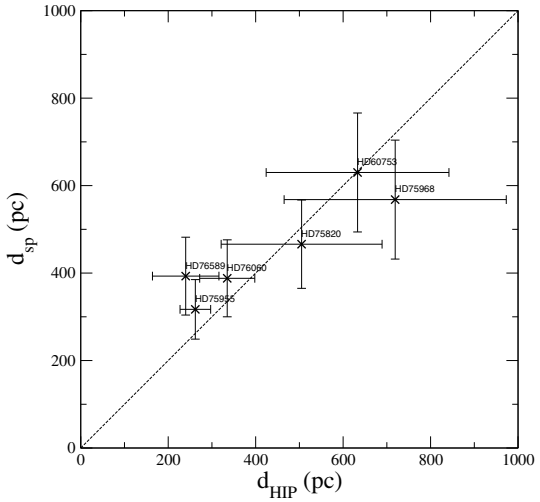

Fig. 3. Distance derived by the method of spectral parallax versus distance according Hipparcos parallax.

their heliocentric radial velocities are given in Table 3. The interstellar absorption lines can be divided into two major groups: low velocity $|V| \lesssim 50$ km s^{-1}, and high velocity $|V| \gtrsim 100$ km s^{-1}. Most stars have one component with a positive radial velocity of ∼22−48 km s^{-1}. The heliocentric velocity can be translated into a LSR velocity in this direction using the relation $V_{\rm LSR} = V_{\rm hel} - 13$ km s^{-1}. This suggests that the dominant population of interstellar clouds in this direction at the distances not exceeding 2 kpc, are characterized by the positive LSR velocities ∼9−35 km s^{-1}. Two stars have negative low velocity components, of −13 km s^{-1} and −46 km s^{-1}.

Three stars have high velocity components: HD 75309 (+153 km s^{-1}, −92 km s^{-1}), HD 76060 (−92 km s^{-1}), and CD-454676 (−150 km s^{-1}). These velocities are typical of high-velocity interstellar Ca II absorption found earlier in the direction of Vela SNR (Cha & Sembach 2000). Interestingly, the spectrum of the star HD 75309 from our program was also studied by Cha & Sembach (2000). Benefitting from the spectrum's high resolution, these authors were able to find eight components including two high velocity components, +136 km s^{-1} and −107 km s^{-1}, and a strong low velocity component +20 km s^{-1}. The corresponding interstellar absorption lines in Table 3 are shifted redward by ≈+16 km s^{-1}, which reflects the systematic difference in radial velocity between the two sets of data. This may be partially related to the low resolution of our spectra. We studied other sources of errors but were unable to explain this disparity.

At least one star, CD-454676, exhibits conspicuous CN absorption of electronic transitions $R(0)$, $R(1)$, and $P(1)$ with the wavelengths of 3873.994 Å, 3874.602 Å, and 3875.759 Å, respectively. The heliocentric radial velocity of these lines is +23 km s^{-1} ($V_{\rm LSR}$ = +10 km s^{-1}), which is consistent with the radial velocity of Ca II interstellar lines in the same star (Table 3). The equivalent width of $R(0)$ and $R(1)$ lines ($W(0)$ = 0.01 Å and $W(1)$ = 0.02 Å) can be used to estimate the excitation temperature of the rotational level $J = 1$ and the column density of CN residing on rotational levels $J = 0$ and $J = 1$ in the weak line limit. Using available oscillator strengths of these transitions (Gredel et al. 2002), we obtain $T = 6.8$ K and column densities $N(0) = 1.34 \times 10^{13}$ cm^{-2} and $N(1) = 1.16 \times 10^{13}$ cm^{-2}. Assuming a Boltzmann population of the $J = 2$ rotational level $N(2) = 5N(0)\exp(-16.325/T)$, we obtain the total CN column density $N = 3.11 \times 10^{13}$ cm^{-2}. These values are comparable to those of CN absorbers towards the Vela OB association (Gredel et al. 2002).

Table 3. Velocities of components of Ca II interstellar absorption.

Star	3933 Å		3968 Å	
	λ(Å)	V (km s^{-1})	λ(Å)	V (km s^{-1})
HD 75309	3935.67	153	3970.53	156
	3934.13	36	3968.91	33
	3933.06	–46	3967.84	–48
	3932.46	–92	3967.23	–94
HD 75820	3933.98	25	3968.76	22
HD 75873	3933.98	25	3968.76	22
HD 75955	3933.95	22	3968.73	19
HD 75968	3933.99	25	3968.76	22
HD 76060	3934.14	36	3968.76	22
	3932.46	–92	3967.23	–94
HD 76589	3934.10	33	3968.88	31
HD 76649	3934.14	36	3968.76	22
HD 76744	3933.95	22	3968.73	19
CD-454590	3934.10	33	3968.88	31
CD-454606	3933.11	34	3968.88	31
	3933.50	–13	3968.27	–15
CD-454645	3934.29	48	3969.07	45
CD-454676	3933.99	25	3968.76	22
	3931.70	–150	3966.47	–151
CD-464666	3934.20	41	3968.87	30

Two stars, HD 75873 and CD-454645, do not exhibit interstellar Ca II lines. In HD 75873 for which $d_{\rm sp}$ = 1400 pc and A_V = 1.2, the expected contribution of the interstellar line to the equivalent width should be about 20%. The explanation of the apparent absence of absorption is the low rotation velocity $V \sin i = 15$ km s^{-1} and the high strength of stellar Ca II absorption. Both factors prevent us from distinguishing interstellar lines in this case. The second star, CD-454645, at a distance of 330 pc is not expected to have strong interstellar Ca II lines. Given its very strong stellar Ca II absorption, the extraction of weak interstellar absorption in this case is precluded.

4. Discussion

4.1. Narrow interstellar lines

Most low velocity interstellar Ca II absorbers with $V_{\rm LSR} \leq 20$ km s^{-1} are most likely produced by local background clouds. This is also true for CN absorbers, which in terms of velocity coincide with the Ca II absorbers. The large scatter in velocities of between −50... and + 30 km s^{-1} exceeding the usual dispersion in cloud velocities of ∼10 km s^{-1} suggests that at least some of these absorbers are related to clouds accelerated by either shock waves driven by wind bubbles of hot stars or old SNR. This conjecture is in accord with results of observations of interstellar ultraviolet O I and Si II absorption lines (Wallerstein et al. 1995) towards the Vela SNR. Some of these lines arise from excited fine-structure levels in the Vela SNR direction and indicate the high pressure of clouds, $p \sim 10^{-10}$ dyn cm^{-2} (Wallerstein et al. 1995), which is two orders of magnitude higher than the average pressure in the interstellar medium (ISM).

The high velocity clouds with $|V_{\rm LSR}| \sim 100$−150 km s^{-1} are probably related to the interstellar clouds shocked by the expanding Vela SNR. Similar high velocity gas was observed in Ca II lines and ultraviolet lines corresponding to different ions, including C I, O I, Mg I, and Mg II (Jenkins & Wallerstein 1995), and attributed to radiative shocks driven by the Vela SNR into

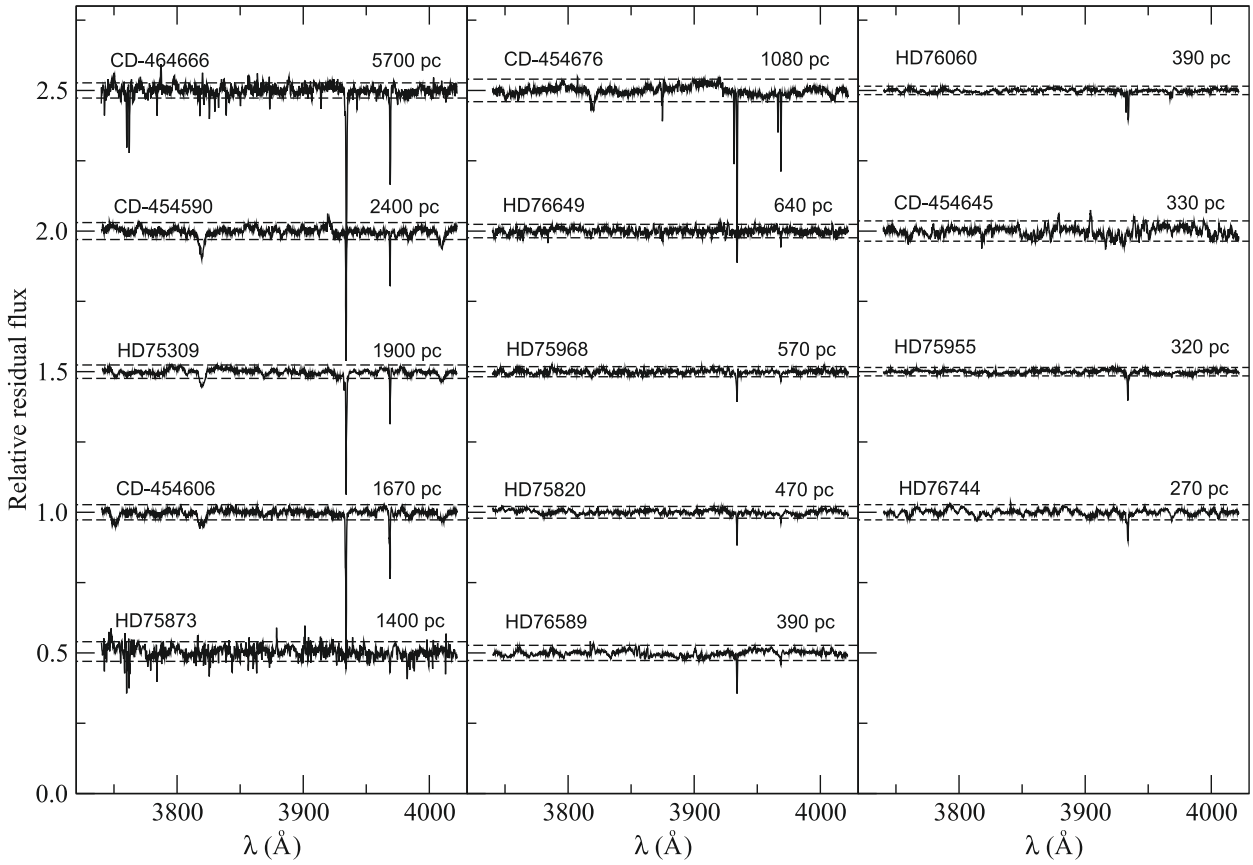

Fig. 4. The relative residual spectra with dashed lines showing the 3σ statistical error boxes varying from ±0.015 to ∼±0.04 from star to star (for 1σ errors in each case, see Table 1). The distance to each star is also indicated.

interstellar clouds of density ∼10 cm^{-3}. Interestingly, the closest star with a high velocity interstellar component, HD 76060, lies at the distance 335 ± 63 pc. This immediately provides an upper limit to the distance of the Vela SNR of ∼335 ± 63 pc, which is consistent with the Vela pulsar distance of 294 pc (Caraveo et al. 2001).

4.2. Broad absorption related to Vela Jr.

The absence of Fe I and Ca II broad absorption lines in stellar spectra towards Vela Jr. requires explanation. As we will see below, singly ionized metals should be more abundantly present in the Vela Jr. ejecta, and therefore absorption by neutral iron, with its relatively low ionization fraction and low value of the oscillator strength, should be significantly weaker than Ca II absorption. We therefore concentrate on the absence of broad Ca II lines. At least four possibilities are conceivable: Vela Jr. is farther than the most distant star in our sample; the SNR is much older; and the Ca II ionization fraction is small, i.e., Ca resides predominantly in the Ca I or in the Ca III ionization state. Discussion of these possibilities requires modeling the broad Ca II absorptions expected at the given age for the remnants of the different SN types.

4.2.1. Broad Ca II absorption for different supernova types

The unshocked ejecta expands freely, i.e., the expansion law at a given age t is $v = r/t$. To describe this we will use cylindrical coordinates (z, p, ϕ) with z-axis coincident with the line of sight directed towards the center of SNR. The absorption produced by the scattering of the background stellar radiation in Ca II 3933, 3968 Å lines at the radial velocity v_z is determined by a Sobolev optical depth in the resonant plane $z = v_z t$ along the line of sight of impact parameter p (assuming that the ejecta is spherically symmetric)

$$\tau(z, p, \phi) = 0.0265 f_{12} \lambda_{12} n_1 t, \quad (5)$$

where the multipliers in the right-hand side in order are oscillator strength, wavelength, Ca II number density at the given radius $r = (z^2 + p^2)^{1/2}$, and the SNR age t.

For a given concentration of Ca determined by the density and Ca abundance, the line strength depends on the ionization fraction of Ca II. At the early phase of the ejecta expansion, at the time of $t \sim 2$ yr after SN explosion, the calcium ionization in ejecta of any type SN is controlled primarily by the ionization loss of fast electrons (Compton electrons and positrons) produced by the radioactive decay chain ^{56}Ni – ^{56}Co – ^{56}Fe and radiative recombination. At the stage of $t \geq 3$ yr, spectra of SNe of different types are dominated by the emission lines of singly ionized metals, which indicates that singly ionized metals dominate. This is supported by numerical models of ionization and thermal balance of ejecta powered by the radioactive decay of ^{56}Co for SN Ia (Axelrod 1980) and SN IIP (Kozma & Fransson 1998). At the later stages $t \sim 10$ yr, the ionization is dominated by positrons from ^{44}Ti decay. Our estimate indicates that even a maximal expected mass 10^{-4} $M_\odot$ of ^{44}Ti is insufficient to maintain the high ionization of Ca. At later stages, therefore, recombination dominates and Ca may become mostly neutral.

However, at the SNR age of $t \sim 10^2$ yr the characteristic recombination time of Ca is larger than the expansion time. At

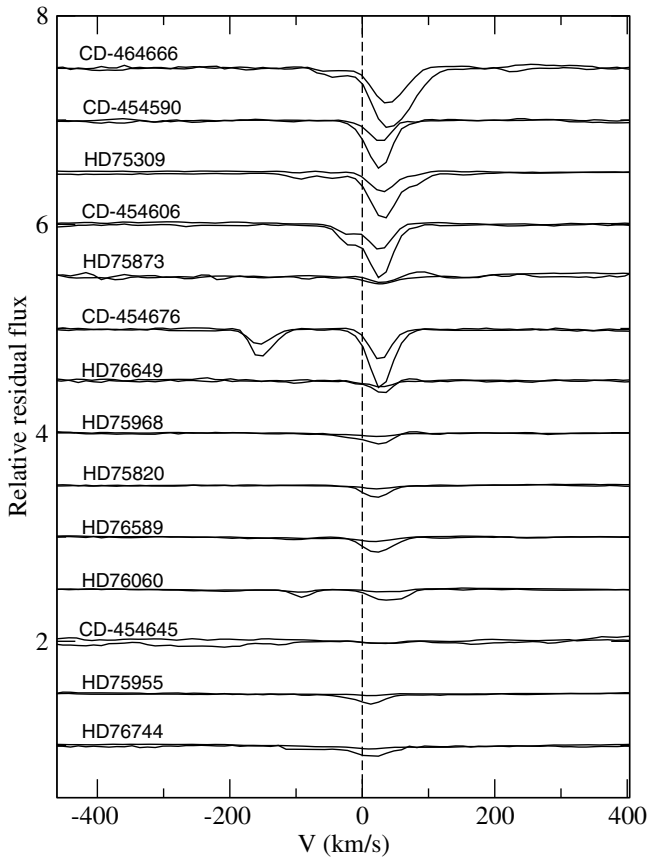

Fig. 5. The relative residual spectra for the stars. The distance increases upward.

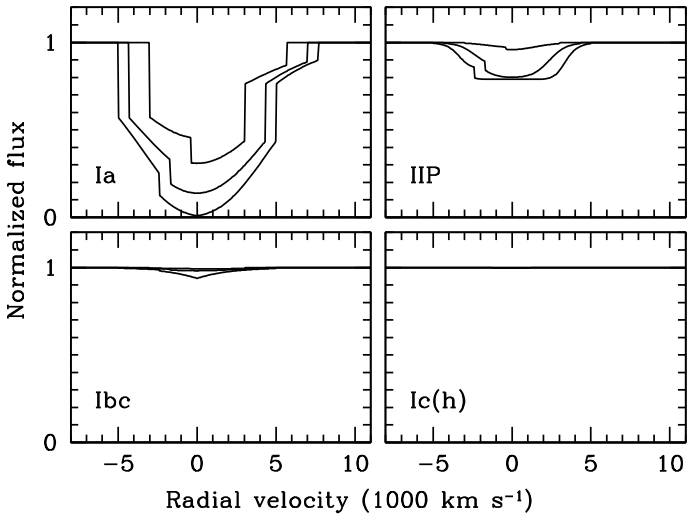

Fig. 6. Absorption profile of Ca II doublet expected in the stellar spectrum of different progenitors of Vela Jr. Shown are cases of impact parameter equal to 0, 0.5, and 0.8. The strongest absorption always corresponds to zero impact parameter.

Table 4. Adopted parameters of supernovae.

Parameters	SN Ia	SN IIP	SN Ibc	SN Ic(h)
M ($M_\odot$)	1.4	10	3	4
E (10^{51} erg)	1.4	1	1.5	20

this stage, the ionization by the starlight may become essential. For example, Fesen et al. (1999) demonstrate that calcium in the ejecta of SN 1885 in M 31 can be efficiently ionized by the bulge starlight within the ionization time of about 10 yr. In the case of Vela Jr. we use the model of the starlight spectrum in the Galactic plane at the radius of 7.5 kpc given by Porter et al. (2006), and the photoionization cross-sections of Verner et al. (1996). The found photoionization time is ~180 yr for Ca I and $\sim 3 \times 10^3$ yr for Ca II. At the age of ~700 yr, we thus expect that Ca in Vela Jr. should be singly ionized.

The ionization of Ca II by X-rays from the reverse shock, and by accelerated protons may also play a role. The X-rays ionize metals from K and L shells, and photoelectrons then ionize Ca II. For the observed X-ray flux $f_x \sim 10^{-10}$ erg cm^{-2} s^{-1} in the 0.5−10 keV band, the characteristic photoionization time for Ca II at the SNR age of 700 yr is found to be $\sim 10^8$ yr for SN Ia, and this process is thus negligible. Ionization by relativistic protons accelerated in the shock wave can be estimated by assuming an average efficiency of cosmic ray acceleration per SN of 10% and the shock wave energy of $\sim 10^{51}$ erg. We find then that the ionization time for Ca II at the age of 700 yr is $\sim 2 \times 10^3$ yr, which is larger than the SNR age. We thus conclude that cosmic rays for the adopted acceleration efficiency essentially cannot ionize Ca II, so all the calcium in the unshocked ejecta of Vela Jr. is expected to remain in Ca II.

The predicted profiles of the Ca II doublet at the age of 700 yr for different varieties of SNe are shown in Fig. 6 assuming that all the calcium is in the Ca II state. We assume that in SN IIP and SN Ibc the Ca abundance is solar, while for SN Ia we assume that the Ca/Fe ratio by mass is solar, while the total mass of iron in the ejecta is 0.6 $M_\odot$. Ejecta parameters for different SNe are given in Table 4. Apart from SN Ia, SN IIP, and SN Ibc, we also consider energetic SN Ic, so-called hypernovae, which is designated hereafter as SN Ic(h). The boundary velocity of the unshocked ejecta is taken to be 5000 km s^{-1} in accordance with the distance of 200 pc and the age of 700 yr. The density distributions $\rho(v)$ in the unshocked ejecta are assumed to be exponential for compact pre-SNe and to form a plateau with the outer power law $\rho \propto v^{-9}$ for SN IIP. The plotted profiles are computed for three values of impact parameter in units of the angular radius: 0, 0.5, and 0.8. The absorption is predicted to be deep for all the impact parameters in the case of SN Ia, rather deep for SN IIP, very weak for SN Ibc, and negligible (relative depth <0.006) in the case of SN Ic(h). If the age and distance of Vela Jr. are close to the values adopted above, the progenitor would be unlikely of type SN Ia or SN IIP; instead an association of the SNR with a SN Ibc or SN Ic(h) is quite plausible.

4.2.2. How far away might Vela Jr. be?

We now relax arguments used earlier to constrain the age and distance of Vela Jr. (Aschenbach 1998; Iyudin et al. 1998) and check whether Vela Jr. lies at a very large distance, >1 kpc, beyond any star in our sample.

For a given ^{44}Ti mass, a combination of age and distance is constrained by the observed flux in the gamma-ray line 1.16 MeV. Nucleosynthesis models predict a production of $(1-5) \times 10^{-5}$ $M_\odot$ of ^{44}Ti in SN Ia (Iwamoto et al. 1998) and $10^{-5}-10^{-4}$ $M_\odot$ in core-collapse SNe (Woosley & Weaver 1995). An independent estimate of the ^{44}Ti yield per SN can be obtained by assuming that almost all the ^{44}Ca is produced as ^{44}Ti both in SN Ia (Iwamoto et al. 1999) and core-collapse SNe (Woosley & Weaver 1995). The solar mass ratio of ^{44}Ca to ^{56}Fe is 10^{-3}, which means that SN IIP and SN Ibc producing 0.05−0.1 of ^{56}Ni

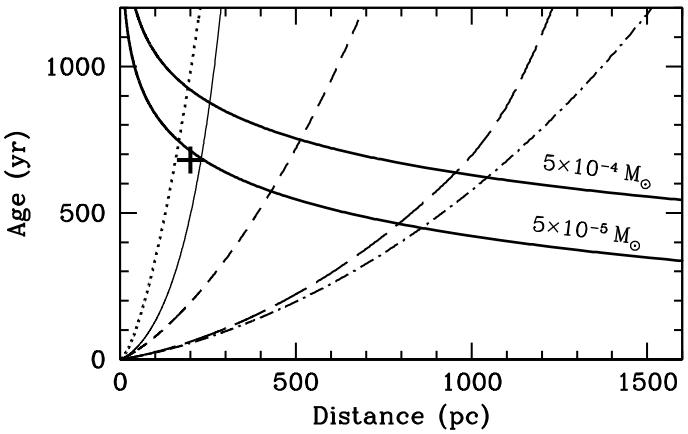

Fig. 7. Age-distance relations provided by ^{44}Ti mass (thick solid lines) and radius of the supernova remnant. The radius is calculated for SN IIP (dotted line), SN Ia (thin solid line), SN Ibc (short-dashed line), SN Ic(h) with 35 $M_\odot$ progenitor (long-dash line), and 60 $M_\odot$ progenitor (dashed-dotted line). Cross shows parameters derived by Iyudin et al. (1998).

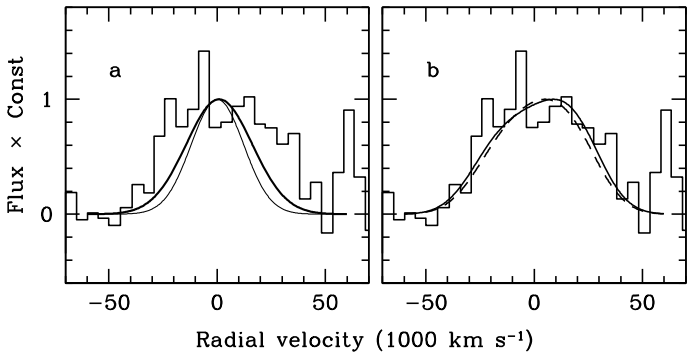

Fig. 8. Profile of 1.16 MeV line of ^{44}Ti. Panel **a)**: profiles for SN Ibc (thin line) and SN Ic(h) (thick line) with spherically-symmetric distribution of ^{44}Ti. Panel **b)**: profiles for SN Ic(h) with ^{44}Ti distributed in the external parts of bi-polar jets at inclination angles of 30° (solid line) and 60° (dashed line).

per SN should eject 5×10^{-5}–10^{-4} $M_\odot$ of ^{44}Ti, while SN Ic(h) producing, in a similar way to SN 1998bw, up to 0.5 $M_\odot$ of ^{56}Ni (Iwamoto et al. 1998) is able to eject as much as $\sim5\times10^{-4}$ $M_\odot$ of ^{44}Ti. We therefore, expect, that the mass of ^{44}Ti ejected by SNe of different types lies in the range 5×10^{-5}–5×10^{-4} $M_\odot$. The corresponding relationship between the age and distance suggested by the observed flux of the 1.16 MeV line 3.8×10^{-5} cm^{-2} s^{-1} is shown in Fig. 7 for the two extreme values of ejected ^{44}Ti mass.

Deceleration of supernova ejecta in the interstellar medium provides us with another relation between the distance and age for a given choice of ejecta parameters, ISM density, and angular radius of Vela Jr. We compute the interaction of ejecta with the ISM in the thin shell approximation (Chevalier 1982) assuming typical ejecta mass and energy (Table 4). In the case of SN IIP, the adopted hydrogen number density of ISM is 0.3 cm^{-3}, which is the average density of the warm neutral medium (WNM). The latter comprises about 80% of the ISM mass (Wolfire et al. 1995). For SN Ia apart from WNM, we also consider the ISM in the form of a hot ionized medium (HIM) of density 0.003 cm^{-3}. This gas occupies about 50–60% of the volume (Wolfire et al. 1995). As in the case of SN Ibc and SN Ic(h), they explode in the ISM modified by the fast main-sequence wind, slow red supergiant wind, and the Wolf-Rayet wind. We consider 35 $M_\odot$ and 60 $M_\odot$ as template progenitor stars; both cases were explored by Garcia-Segura et al. (1996). According to these results the pre-SN in the 35 $M_\odot$ case is imbedded in a hot bubble of the uniform density of ~0.003 cm^{-3} with a radius of 18 pc surrounded by a dense cool shell of total mass ~20 $M_\odot$. For the 60 $M_\odot$ progenitor, the bubble density is ~0.001 cm^{-3} and its radius is 50 pc. We note in passing that a model of Vela Jr. (RXJ0852.0-4622) taken to be of the SNII/Ib type exploded in a wind blown cavity was considered by Berezhko et al. (2009).

The age-distance relations for all the discussed cases are shown in Fig. 7. The SN Ia exploded in the HIM phase shows almost the same age-distance relation as SN Ibc and is therefore not shown in this figure. This diagnostic plot is similar to that used by Chen & Gehrels (1999). The essential difference, however, is that they used a set of arbitrary expansion velocities of the swept-up shell, while we calculate the evolution of the shell radius for each type of SN. For a given age, the minimal distance corresponds to a SN IIP expanding in the WNM phase, while the maximal distance corresponds to a SN Ic(h) with a 60 $M_\odot$ progenitor. In combination with the ^{44}Ti curves, these two cases imply the allowed ranges of 450–900 yr and 150–1000 pc for the age and distance of Vela Jr., respectively. The major result of this plot is that the distance of Vela Jr. cannot exceed 1 kpc. We thus conclude that at least several stars in our sample (Table 2) are behind the SNR. This permits us to disregard the explanation of the absence of broad Ca II absorption being the result of the large distance to Vela Jr.

4.2.3. Was the progenitor of Vela Jr. a hypernova?

The absence of broad Ca II absorption in the spectra of stars at distances >1 kpc suggests that the SNR progenitor was either of SN Ibc or SN Ic(h) because only for these SNe is the expected absorption weak and possibly undetected (Fig. 6). To distinguish between these two SN possibilities, one should take into account the intrinsic width of the 1.16 MeV line.

In the case of SN Ibc at the age of 650 yr, the expected profile of the ^{44}Ti line (cf. Fig. 7) convolved with the instrumental profile (σ = 45 keV) is found to be too narrow compared with the observed one (Fig. 8a), even assuming homogeneous mixing of ^{44}Ti up to a velocity of 10 000 km s^{-1}. The observed broad profile of the 1.16 MeV line implies that most of the ejecta mass consisting of ^{44}Ti has significantly larger velocities. However, the SN Ic(h) case with maximal expansion velocities of 31 300 km s^{-1}at the age of ~500 yr (the case of 60 $M_\odot$) and spherically-symmetric distribution of ^{44}Ti homogeneously mixed to 31 000 km s^{-1} does not help resolve the ambiguity either (Fig. 8a).

The solution to the line width problem might be found by taking into account that iron-peak elements are ejected by SN Ic(h) in the form of high velocity bipolar jets and assuming that ^{44}Ti resides only in the outer parts of the jets. ^{56}Ni-rich bipolar jets are predicted by the collapsar model (MacFadyen & Woosley 1999) proposed for the hypernova SN 1998bw, and the jet-like structure is consistent with the spectral line profiles (Maeda et al. 2006). Maeda & Nomoto (2003) also predict an external location of ^{44}Ti. In the 1.16 MeV profile simulations, we assume that ^{44}Ti is homogeneously distributed along the radius in the velocity range of 20 000–31 000 km s^{-1} within jets of opening angle 60° and inclination angle θ. We took into account the light travel-time delay that produces the profile skewed towards red. Two cases are shown (Fig. 8b) for the angle between the jet axis and the line of sight, θ = 30° and θ = 60°, both of which fit the data more closely than the spherically symmetric model. We therefore conclude that the hypernova model with

the outer location of ^{44}Ti in bipolar jets of SN Ic(h) is consistent both with the absence of the broad Ca II absorption, and the broad 1.16 MeV profile.

A problem with the SN Ic(h) scenario is that the high ejecta velocity implied by this model infers a low ambient density, which seems to disagree with the baryonic origin of TeV gamma-ray emission from Vela Jr. Gamma ray production via *pp*-collisions seems to be the preferred model compared to the inverse Compton mechanism (Aharonian et al. 2005; Berezhko et al. 2009). An alternative may be provided by assuming that we see the early stage of the interaction of the SNR with a dense environment that has not yet been affected by the previous expansion dynamics. This conjecture is in line with the low expansion velocity found for the NW rim by Katsuda et al. (2008). Another discomfort is related to the hypernova being a rare variety of SNe that comprises only about 1% of all SNe Ibc (Podsiadlowski et al. 2004). Only high signal-to-noise spectral imaging of Vela Jr. in the 1.16 MeV line band with energy resolution of $\leq$40 keV and angular resolution of $\leq 1^\circ$ may confirm (or reject) the high velocities of ^{44}Ti and detect any jet-like (if any) structure of the ^{44}Ti distribution.

Given the difficulties arising in the interpretation of data on Vela Jr., we should not exclude out completely the possibility that this SNR is older (Katsuda et al. 2008). However, only additional observations at different wavelength bands will be able to help pinpoint the age and the origin of Vela Jr.

5. Conclusions

We have presented our attempt to detect unshocked ejecta of the young SNR Vela Jr. by analyzing broad Ca II absorption lines in spectra of background stars. We obtained and analyzed spectra of 14 stars across Vela Jr. using standard methods of spectral synthesis. We concluded that broad absorption lines are absent. The 3σ upper limit to the depth of broad absorption lines is 0.04. We detected both low velocity and high velocity interstellar Ca II absorptions. The latter are attributed to the cold gas of radiative shocks propagating in clouds engulfed by the old Vela SNR.

The absence of broad Ca II absorption lines and the constraints imposed by the flux of the ^{44}Ti gamma-ray line and the angular size of the SNR imply that only SN Ibc or energetic SN Ic (hypernovae) could have produced Vela Jr., if our estimates of the age and distance are correct. The additional constraint provided by the width of the 1.16 MeV ^{44}Ti line also supports the hypernova scenario for Vela Jr. origin. However, we emphasize the need for more reliable data on the ^{44}Ti gamma-ray line profile and higher resolution imaging of Vela Jr. in the gamma line to verify the hypernova scenario.

References

Aharonian, F., Akhperjanian, A. G., Bazer-Bachi, A. R., et al. 2005, A&A, 437, L7
Aschenbach, B. 1998, Nature, 396, 141
Aschenbach, B., Iyudin, A. F., & Schönfelder, V. 1999, A&A, 350, 997
Axelrod, T. S. 1980, Ph.D. Thesis (California Univ., Santa Cruz.)
Bamba, A., Yamazaki, R., & Hiraga, J. S. 2005, ApJ, 632, 294
Berezhko, E. G., Pühlhofer, G., & Völk, H. J. 2009, A&A, 505, 641
Bessell, M. S., Castelli, F., & Plez, B. 1998, A&A, 333, 231
Caraveo, P. A., De Luca, A., Mignani, R. P., & Bignami, G. F. 2001, ApJ, 561, 930
Carroll, J. A. 1933, MNRAS, 93, 478
Castelli, F., & Kurucz, R. L. 2003, in Modelling of Stellar Atmospheres, ed. N. Piskunov, W. W. Weiss, & D. F. Gray, IAU Symp., 210, 20
Cha, A. N., & Sembach, K. R. 2000, ApSS, 126, 399
Chen, W., & Gehrels, N. 1999, ApJ, 514, L103
Chevalier, R. A. 1982, ApJ, 259, 302
Duncan, A. R., & Green, D. A. 2000, A&A, 364, 732
Fesen, R. A., Saken, J. M., & Hamilton, A. J. S. 1989, ApJ, 341, L55
Fesen, R. A., Gerardy, C. L., McLin, K. M., & Hamilton, A. J. S. 1999, ApJ, 514, 195
Garcia-Segura, G., Langer, N., & Mac Low, M. 1996, A&A, 316, 133
Gredel, R., Pineau des Forêts, G., & Federman, S. R. 2002, A&A, 389, 993
Hamilton, A. J. S., Fesen, R. A., Wu, C., Crenshaw, D. M., & Sarazin, C. L. 1997, ApJ, 481, 838
Hamilton, A. J. S., Fesen, R. A., & Blair, W. P. 2007, MNRAS, 381, 771
Iwamoto, K., Mazzali, P. A., Nomoto, K., et al. 1998, Nature, 395, 672
Iwamoto, K., Brachwitz, F., Nomoto, K., et al. 1999, ApJSS, 125, 439
Iyudin, A. F., Schönfelder, V., Bennett, K., et al. 1998, Nature, 396, 142
Jenkins, E. B., & Wallerstein, G. 1995, ApJ, 440, 227
Katsuda, S., Tsunemi, H., & Mori, K. 2008, ApJ, 678, L35
Kozma, C., & Fransson, C. 1998, ApJ, 496, 946
Kurucz, R. 1993, ATLAS9 Stellar Atmosphere Programs and 2 km s^{-1} grid. Kurucz CD-ROM (Cambridge, Mass.: Smithsonian Astrophysical Observatory), 13
MacFadyen, A. I., & Woosley, S. E. 1999, ApJ, 524, 262
Maeda, K., & Nomoto, K. 2003, ApJ, 598, 1163
Maeda, K., Mazzali, P. A., & Nomoto, K. 2006, ApJ, 645, 1331
Mathis, J. S. 1990, ARA&A, 28, 37
Podsiadlowski, P., Mazzali, P. A., Nomoto, K., Lazzati, D., & Cappellaro, E. 2004, ApJ, 607, L17
Porter, T. A., Moskalenko, I. V., & Strong, A. W. 2006, ApJ, 648, L29
Schaller, G., Schaerer, D., Meynet, G., & Maeder, A. 1992, A&ASS, 96, 269
Slane, P., Hughes, J. P., Edgar, R. J., et al. 2001, ApJ, 548, 814
Tsymbal, V., Lyashko, D., & Weiss, W. W. 2003, in Modelling of Stellar Atmospheres, ed. N. Piskunov, W. W. Weiss, & D. F. Gray, IAU Symp., 210, 49
van Leeuwen, F. 2007, A&A, 474, 653
Verner, D. A., Ferland, G. J., Korista, K. T., & Yakovlev, D. G. 1996, ApJ, 465, 487
Wallerstein, G., Vanture, A., & Jenkins, E. B. 1995, ApJ, 455, 590
Winkler, P. F., Long, K. S., Hamilton, A. J. S., & Fesen, R. A. 2005, ApJ, 624, 189
Wolfire, M. G., Hollenbach, D., McKee, C. F., Tielens, A. G. G. M., & Bakes, E. L. O. 1995, ApJ, 443, 152
Woosley, S. E., & Weaver, T. A. 1995, ApJSS, 101, 181